JOURNAL OF BACTERIOLOGY, Feb. 2006, p. 1011–1021 Vol. 188, No. 3
0021-9193/06/$08.00+0 doi:10.1128/JB.188.3.1011–1021.2006

Native Cell Wall Organization Shown by Cryo-Electron Microscopy Confirms the Existence of a Periplasmic Space in *Staphylococcus aureus*

Valério R. F. Matias* and Terry J. Beveridge

Biophysics Interdepartmental Group and Department of Molecular and Cellular Biology, College of Biological Science, University of Guelph, Guelph, Ontario, Canada N1G 2W1

Received 27 September 2005/Accepted 14 November 2005

The current perception of the ultrastructure of gram-positive cell envelopes relies mainly on electron microscopy of thin sections and on sample preparation. Freezing of cells into a matrix of amorphous ice (i.e., vitrification) results in optimal specimen preservation and allows the observation of cell envelope boundary layers in their (frozen) hydrated state. In this report, cryo-transmission electron microscopy of frozen-hydrated sections of *Staphylococcus aureus* D_2C was used to examine cell envelope organization. A bipartite wall was positioned above the plasma membrane and consisted of a 16-nm low-density inner wall zone (IWZ), followed by a 19-nm high-density outer wall zone (OWZ). Observation of plasmolyzed cells, which were used to artificially separate the membrane from the wall, showed membrane vesicles within the space associated with the IWZ in native cells and a large gap between the membrane and OWZ, suggesting that the IWZ was devoid of a cross-linked polymeric cell wall network. Isolated wall fragments possessed only one zone of high density, with a constant level of density throughout their thickness, as was previously seen with the OWZs of intact cells. These results strongly indicate that the IWZ represents a periplasmic space, composed mostly of soluble low-density constituents confined between the plasma membrane and OWZ, and that the OWZ represents the peptidoglycan-teichoic acid cell wall network with its associated proteins. Cell wall differentiation was also seen at the septum of dividing cells. Here, two high-density zones were sandwiched between three low-density zones. It appeared that the septum consisted of an extension of the IWZ and OWZ from the outside peripheral wall, plus a low-density middle zone that separated adjacent septal cross walls, which could contribute to cell separation during division.

Staphylococcus aureus is a gram-positive pathogen often involved in nosocomial infections and food-borne diseases, and there is now growing concern about the spread of multidrug-resistant strains of methicillin-resistant *S. aureus* (4, 25, 26, 31, 39, 45). The staphylococcal cell wall plays an important role for this organism's success, as it withstands tremendous turgor pressures throughout the cell cycle (ca. 20 to 30 atm), strongly interacts with the cell's external environment, particularly in infection processes, and is intimately involved in cell division (1–3, 15, 21, 22, 33). Over the past two decades much knowledge has been accumulated on the primary structure of staphylococcal cell wall components, i.e., peptidoglycan (3, 15, 45), (lipo)teichoic acids (34, 47, 48), and surface proteins (33, 43), but there is still a lack of structural information at high resolution on the spatial organization of this complex cell wall (4, 9, 17, 46, 49).

As with other gram-positive bacteria, the envelope of *S. aureus* is commonly seen in conventional thin sections by electron microscopy as composed of a plasma membrane tightly bound by a thick and undifferentiated wall (Fig. 1). This simple architecture has been attributed to the harsh procedures required to produce resin embeddings (4, 5). Chemical fixation, dehydration, heavy metal staining, and plastic embedding introduce many artifacts, which are aggravated by long treatment times. Rapid freezing used as a fast physical means of fixation, in combination with the simultaneous dehydration and chemical fixation at low temperatures in the freeze-substitution method, has provided better preservation of staphylococci for transmission electron microscopy (TEM) of thin sections (4, 44, 47, 49). Such thin sections of *S. aureus* provide more structural detail than conventional sections do and show a tripartite cell wall surrounding the membrane. A highly stained thin inner zone (region 1) is enclosed by a low-contrast thicker region (region 2) and is followed by a more fibrous wall (region 3) (Fig. 2). This is similar to the layering seen in the freeze-substituted cell wall of *Bacillus subtilis* (16, 17). However, this arrangement must be attributed to dissimilar wall architectures, since in *B. subtilis* the three-zoned wall reflects the way the cell wall turns over, whereas in *S. aureus* wall growth proceeds differently, as explained below.

Cell elongation in the rod-shaped bacterium *B. subtilis* proceeds with the insertion of newer wall material on the inner face of the cylindrical wall, which is pushed outwards and stretched because of cellular turgor pressure (and becomes the middle zone). Older material on the outer surface is fragmented into fibers, due to the action of autolysins, and is shed (3, 20). New wall material progresses through the wall from inside to outside as the wall matures and is finally excised. The translucent and fibrous walls seen in freeze-substituted *B. subtilis* are consistent with the reactive sites for heavy metal binding with fully intact and partially degraded walls, respectively (16, 17). In contrast, the staphylococcal wall grows predominantly with the insertion of new wall material at division sites in the middle of the cell, forming a cross wall or growing septum, which eventually fuses to develop a complete septum

* Corresponding author. Mailing address: Department of Molecular and Cellular Biology, College of Biological Science, University of Guelph, Guelph, Ontario, Canada N1G 2W1. Phone: (519) 824-4120, ext. 58904. Fax: (519) 837-1802. E-mail: vmatias@uoguelph.ca.

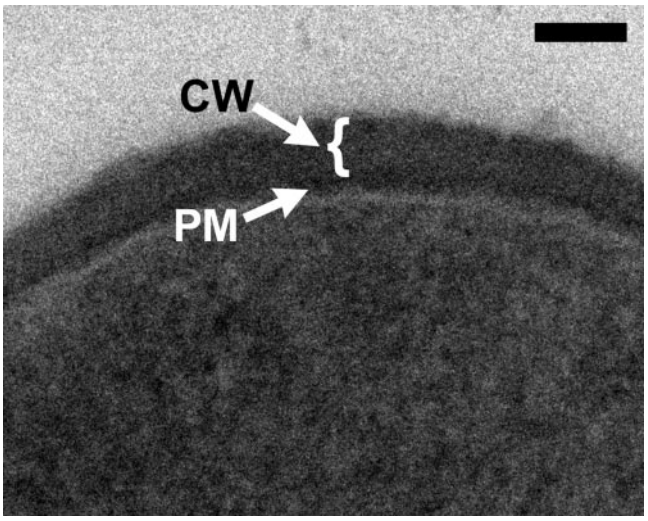

FIG. 1. Thin section of the cell envelope of a conventionally embedded *Staphylococcus aureus* D_2C. The plasma membrane (PM) appears tightly bound by a thick and amorphous cell wall (CW). Bar, 50 nm.

(1, 2, 15, 21). In *S. aureus*, autolysins have hitherto been localized only at the septum, where they have been implicated in splitting the cross wall into two leaflets, each leaflet forming one hemisphere of the newly generated daughter cells (15, 53). Since wall synthesis and (eventually) autolytic activity are associated with the septum, new wall materials do not seem to be incorporated into the cell wall of *S. aureus* by an inside-to-outside mechanism.

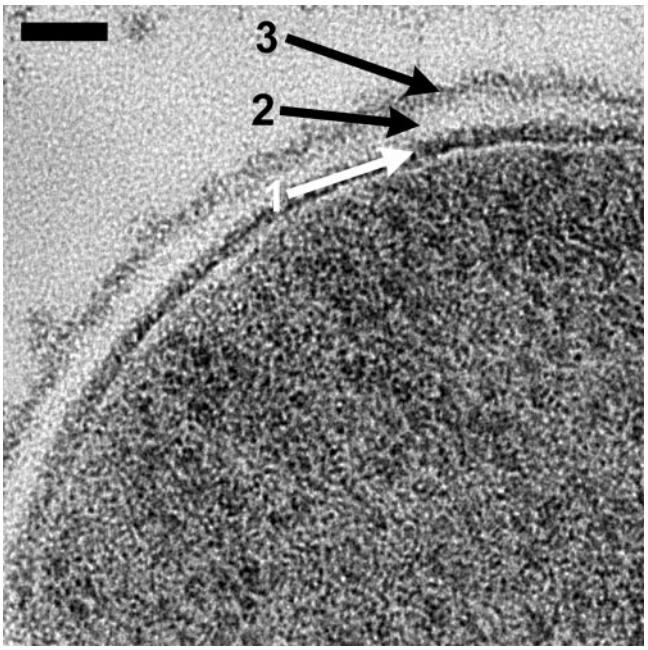

FIG. 2. Thin section of the cell envelope of a freeze-substituted cell. A tripartite wall is seen enclosing the plasma membrane: 1, heavily stained inner thin zone; 2, intermediate translucent region; 3, outer highly stained fibrous surface. Region 1 is so heavily stained that visualization of the plasma membrane is difficult. The plasma membrane resides immediately below this heavily stained layer of the wall (17). Bar, 50 nm.

The tripartite wall displayed in freeze-substituted *S. aureus* has been interpreted as defining the segregation of components within the wall. Freeze-substitution of isolated cell walls, in combination with immunogold labeling, has indicated that the fuzzy coat of *S. aureus* wall consists mostly of teichoic acids (47). The existence of a periplasmic space has been proposed to explain the heavily stained thin zone adjacent to the membrane (44, 47). Although structural preservation is better achieved by freeze-substitution, we believe specimen dehydration and heavy metal staining can still cause perturbations of the native wall conformation.

In this report, cryo-TEM of frozen-hydrated sections is used to further evaluate staphylococcal cell wall organization. Here, immobilization of structures at the molecular level is achieved by vitrifying samples within a matrix of amorphous ice, resulting in optimal structural preservation. Chemical fixatives and heavy metal stains are not used, and after vitrification, samples are kept in their hydrated state for viewing. Vitrified specimens are cryo-sectioned, and cells in frozen sections are observed at low temperatures by cryo-TEM with the aid of phase contrast (12, 29). Production of frozen-hydrated sections is the most difficult step of the technique, but advances in the sectioning apparatus and high-pressure freezing have improved results (11, 29, 37, 42, 54). This approach has recently resulted in optimal structural preservation of bacteria and has allowed the observation of a periplasmic space in *B. subtilis* as a model gram-positive bacterium (30). Motivated by this result, we have investigated the polymeric network of the wall and the possible existence of a periplasmic space in *S. aureus* as an example of an important pathogen, especially since this gram-positive bacterium's mode of wall expansion and cell growth differs substantially from that of *B. subtilis*.

MATERIALS AND METHODS

Bacterial strains and growth conditions. *S. aureus* Newman D_2C and *B. subtilis* 168 were grown at 37°C to a mid-exponential growth phase (optical density at 470 nm, 0.5 to 0.8) in either Trypticase soy broth (TSB) or TSB containing 10% (wt/wt) glycerol (used as a cryoprotectant). Harvested cells (centrifuged at 6,000 × *g* for 5 min) were washed three times in 50 mM HEPES (pH 7.0) or in 10 mM HEPES containing 10% (wt/wt) glycerol. The pellet of cells grown in TSB with glycerol and washed in buffered glycerol was directly used for freezing.

Isolation of cell wall fragments. *S. aureus* grown in TSB was resuspended in 50 mM HEPES (pH 7.0) containing 50 mg/ml DNase and 50 mg/ml RNase, and 0.5-ml aliquots of the pellet were added to 1.5 ml of 0.1-mm zirconia/silica beads in 2-ml tubes. Bacteria were mechanically broken by two 1-min agitations at 4,600 rpm in a Bead Beater (Biospec), with cooling of the tubes on ice between agitations. The supernatant was centrifuged to remove intact cells and residual beads (3,000 × *g*). The remaining supernatant, containing the cell wall fragments, was boiled in 4% (wt/vol) sodium dodecyl sulfate (SDS) for 2 h (41). For the extraction of teichoic acids (TA), water-washed cell wall fragments were treated with 10% (wt/vol) trichloroacetic acid for 2 h at 60°C (19). Further, water-washed TA-extracted cell walls were incubated in a protease solution (500 μg/ml α-chymotrypsin in 50 mM HEPES [pH 7.2] containing 10 mM $CaCl_2$) for 2 h at 30°C to remove any remaining protein associated with the wall. Protease-treated walls were then boiled in 4% SDS for 1 h to remove any remaining protease. All wall fragments were washed five more times in deionized water and three times in 17.5% (wt/wt) glycerol in 10 mM HEPES (pH 7) for freezing.

Plasmolysis experiment. In order to plasmolyze D_2C cells, 1 ml of the pellet was resuspended in 40 ml of either 10, 20, 25% (wt/vol) NaCl, or 10% NaCl containing 10% (wt/vol) glucose, all prepared in 10 mM HEPES (pH 7.0). In all cases, the concentration of the salt was sufficient to provide cryoprotection. Pellets obtained were used for freezing.

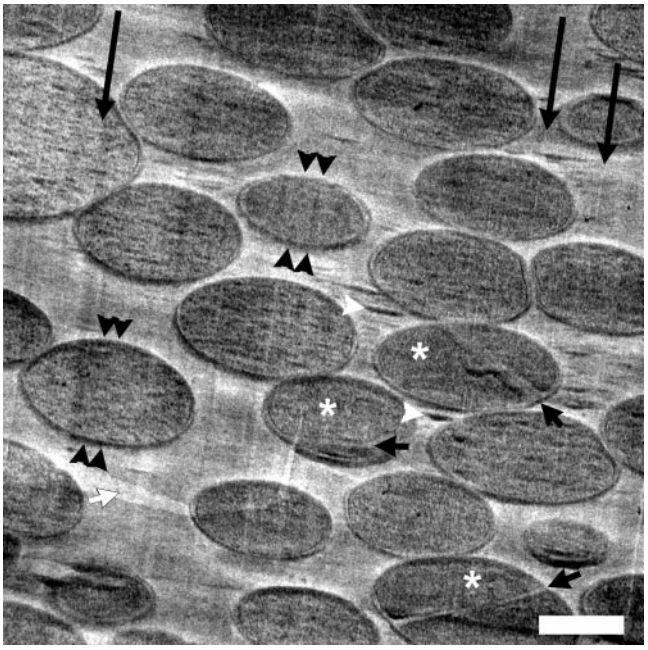

FIG. 3. Energy-filtered image of a frozen-hydrated section of *S. aureus* D_2C at low magnification. Long arrows point to knife marks, white arrowheads to crevasses, double black arrowheads to compression in the cutting direction (this is why cells look more oblong than circular), and a short white arrow to a crack in the supporting film. White asterisks indicate cells possessing a septum, and short black arrows point to the septa. Bar, 500 nm.

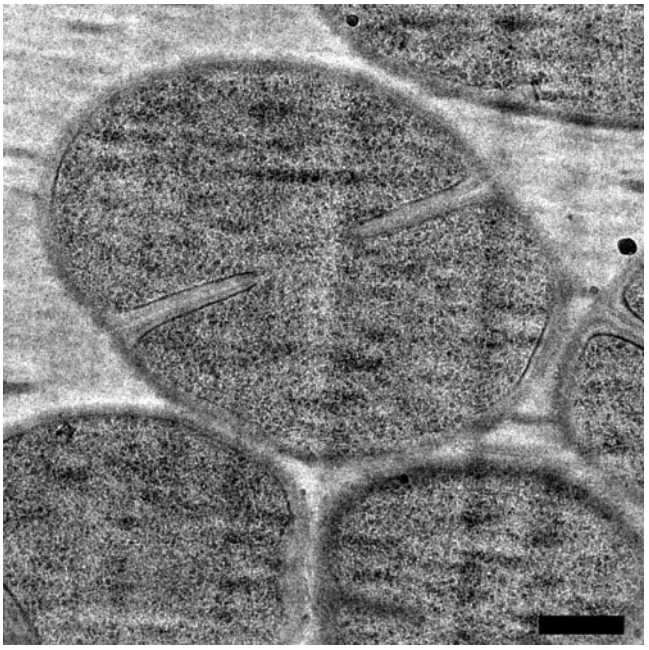

FIG. 4. Frozen-hydrated section of *S. aureus* D_2C at intermediate magnification. Ribosomes (seen as dense 20-nm particles) are evenly disbursed throughout the cytoplasm, which appears without visible aggregation of DNA. The cell at the middle of the figure is dividing and has a septum. Bar, 200 nm.

Freezing and sectioning of bacteria. Bacteria and cell wall fragments were frozen and sectioned as previously described (30). Briefly, pellets of samples for freezing were drawn into a disposable plastic syringe, and bacteria or walls were injected into copper tubes from the syringe and immediately vitrified using a Leica EM PACT high-pressure freezer (for details on high-pressure freezing, see references 32 and 37). Frozen samples were sectioned in a Leica cryo-ultramicrotome and mounted on carbon-coated 1500-mesh copper grids.

Conventional embedding and freeze-substitution. Cells for conventional embedding were prepared as described by Beveridge et al. (5). For freeze-substitution, copper tubes with frozen cells were cut, under liquid nitrogen, into roughly 2-mm-long pieces. These pieces were transferred to small vials containing 0.5 ml of freeze-substitution medium (2% osmium tetroxide and 2% uranyl acetate in anhydrous ethanol), and vials were transferred to a Leica automatic freeze-substitution apparatus. Freeze-substitution was carried out at −90°C for 18 h, at −60°C for 15 h, and at −30°C for 12 h, and then the temperature was slowly ramped up to room temperature over an 18-h period. Cells were washed in ethanol, embedded in LR White (London Resins), thin sectioned at room temperature, and sections were poststained with uranyl acetate and lead citrate (17).

Cryo-TEM and chemical analyses. Grids containing the frozen-hydrated thin sections were mounted into a Gatan cryo-holder for direct observation at −170°C in a LEO 912AB energy-filtered cryo-TEM operating at 120 kV. Energy filtering improves image contrast by eliminating inelastically scattered electrons, which causes a blurring effect on micrographs. Zero-loss energy-filtered images were taken using a slow-scan charge-coupled device camera (Proscan) (1,024 × 1,024 pixels). Freeze-substituted cells were observed at room temperature, under the same operating conditions. Images were stored and analyzed using analySIS software (SIS, Munster, Germany). Length measurements were done on the least deformed regions of frozen-hydrated cells (29, 30).

Phosphorous analysis of cell walls was performed using a Varian Vista-pro radial induction-coupled plasma spectrometer with a Cetac ultrasonic nebulizer. Muramic acid, aspartic acid, and threonine analyses were carried out by high-performance cation-exchange chromatography using a Beckman system Gold amino acid analyzer (7). Phosphorus, muramic acid, and the amino acids threonine and aspartic acid were used as markers for teichoic acid, peptidoglycan, and protein, respectively.

RESULTS

Freezing, sectioning, and cutting artifacts. *S. aureus* grown in the presence of 10% (wt/wt) glycerol was consistently vitrified by high-pressure freezing. Growth in the presence of the cryoprotectant was chosen so as to minimize osmotic effects on cells, and compared to growth without glycerol, there was little change in the growth rate (doubling time of 35 min for glycerol versus doubling time of 30 min without glycerol).

Low-magnification micrographs of *S. aureus* showed the cutting artifacts commonly associated with frozen-hydrated sections (Fig. 3). Unlike resin-embedded samples, which use the surface tension of water to stretch and float sections during sectioning, frozen-hydrated sections are produced on a dry knife. Hence, tensional stresses created during sectioning remain on the sections, leaving artifacts on them. Cutting artifacts can nevertheless be systematically taken into account, as they are all related to the cutting direction. These artifacts include knife marks, crevasses, compression along the cutting direction, and ice crystal contamination (for a detailed discussion on cutting artifacts, see references 12, 29, and 30). Previous work on rod-shaped bacteria also faced an additional problem. Freezing of concentrated cell pellets in capillary copper tubes caused the alignment of cells along the length of the tubes, preventing the observation of longitudinal sections. Here, due to the spherical shape of *S. aureus*, cells were found randomly aligned on the sections, and frequent observation of cell division was therefore possible (Fig. 3).

Frozen-hydrated *S. aureus* and its cell wall organization. Frozen-hydrated sections of *S. aureus* showed cytoplasm filled with evenly dispersed ribosomes without visible aggregation of DNA (Fig. 4). The cell wall was well preserved at the least

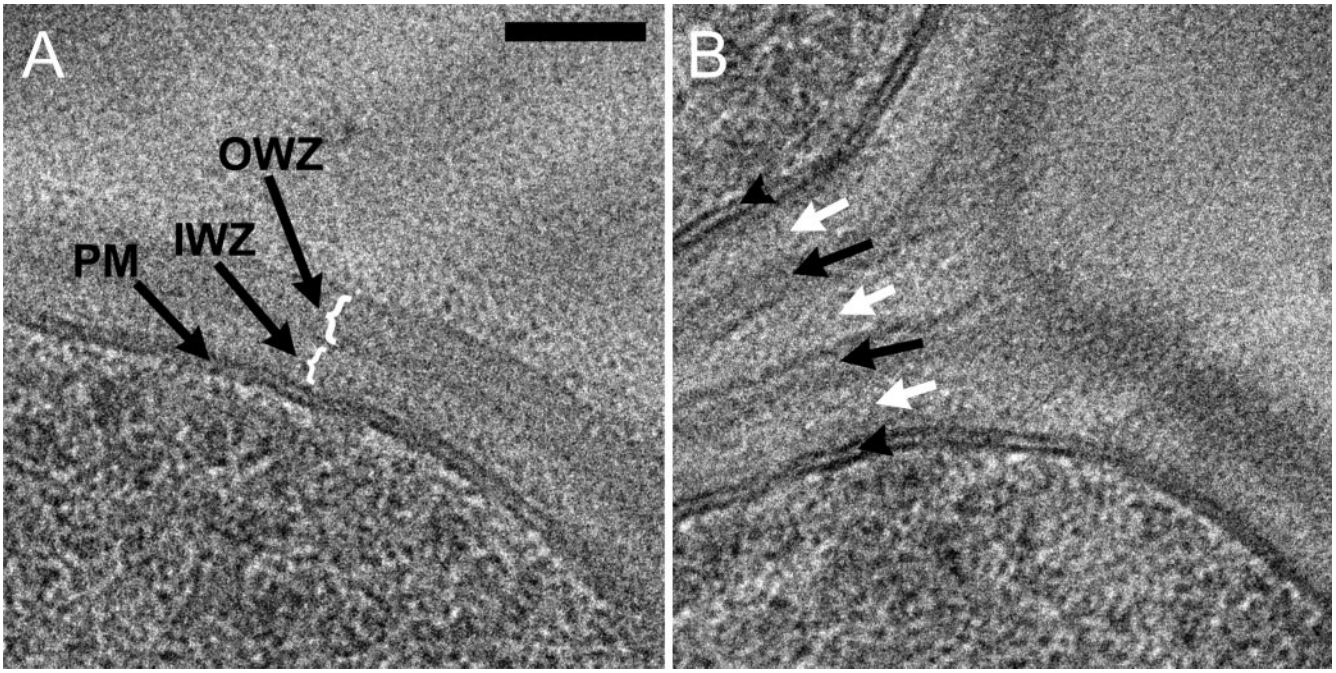

FIG. 5. Frozen-hydrated section at high magnification showing the *S. aureus* cell envelope. (A) At nonseptal regions, the plasma membrane (PM) is bound by a bipartite wall; a low-density inner wall zone (IWZ) precedes a high-density outer wall zone (OWZ). (B) At the septum, five different zones of alternating low (white arrows) and high (black arrows) densities are distinguished between the two membranes of the septum (arrowheads). Both images are shown at the same magnification. Bar, 50 nm.

compressed regions of cells (30), where the plasma membrane appeared bounded by a two-zoned wall at nonseptal regions (Fig. 5A). A 16-nm inner wall zone (IWZ) showing low contrast preceded a high-contrast 19-nm outer wall zone (OWZ) (Table 1 and Fig. 5A). Since in frozen-hydrated samples, contrast is directly proportional to density, this bipartite view of the staphylococcal wall represents regions of different distinct densities (12). Although a bipartite staphylococcal wall differs from the tripartite wall seen in freeze-substituted specimens, it resembles the *B. subtilis* wall seen in frozen-hydrated sections (30, 44, 47).

At the septum, five zones of alternating densities were observed between the membranes of the two daughter cells, with two high-density zones appearing to be sandwiched by three low-density zones (Fig. 5B). This septal profile is markedly different compared to both conventional embeddings and freeze-substituted results of *S. aureus*, which show a heavily stained midline at the cross wall (4, 15, 44, 46). Nevertheless, the two zones next to the membrane at the septum seemed to be an extension of the bipartite wall of the cell wall envelope (cf. Fig. 5A and B). This will be discussed in more detail below.

Plasmolysis experiments. In order to help distinguish the constitution of each wall zone seen in the *S. aureus* envelope, cells were osmotically shocked to artificially separate the membrane from the walls. For this purpose, cells grown without a cryoprotectant were subjected to a high-osmolarity solution. Solutions of 20 and 25% NaCl gave the best plasmolysis results, but the high concentration of salts made it difficult to obtain sections without pronounced cutting artifacts, necessary for higher image resolution (not shown). Plasmolysis was still achieved after incubation in a solution of 10% NaCl containing 10% glucose, and the presence of glucose seemed to improve section quality. It is possible that the glucose acted as both an osmolyte and cryoprotectant. The high osmolarities necessary to plasmolyze *S. aureus* reflect the high osmotolerance of this organism, which is able to grow over a wide range of osmotic

TABLE 1. Measurements of structures and compartments of *S. aureus* D_2C[a]

Structure or compartment measurement	Cells	Cell wall fragments	Teichoic acid-extracted wall fragments	Protein-and-teichoic acid-extracted walls	Plasmolyzed cells
Cell or cylinder diam (μm)[b]	1.05 ± 0.07	NA[c]	NA	NA	0.98 ± 0.15
Protoplast diam (μm)	0.97 ± 0.07	NA	NA	NA	0.85 ± 0.14
Plasma membrane thickness (nm)	5.4 ± 0.4	NA	NA	NA	5.5 ± 1.5
Inner wall zone thickness (nm)	15.8 ± 2.5	NA	NA	NA	NA[d]
Outer wall zone thickness (nm)	19.0 ± 4.3	32.8 ± 4.1	32.5 ± 5.5	33.8 ± 5.4	30.3 ± 5.1

[a] Values are the averages ± standard deviations of 12 measurements.
[b] Taken across the cell from the outer face to the outer face of the wall.
[c] NA, not applicable.
[d] The uneven spacing of the inner wall zone made measurement impossible.

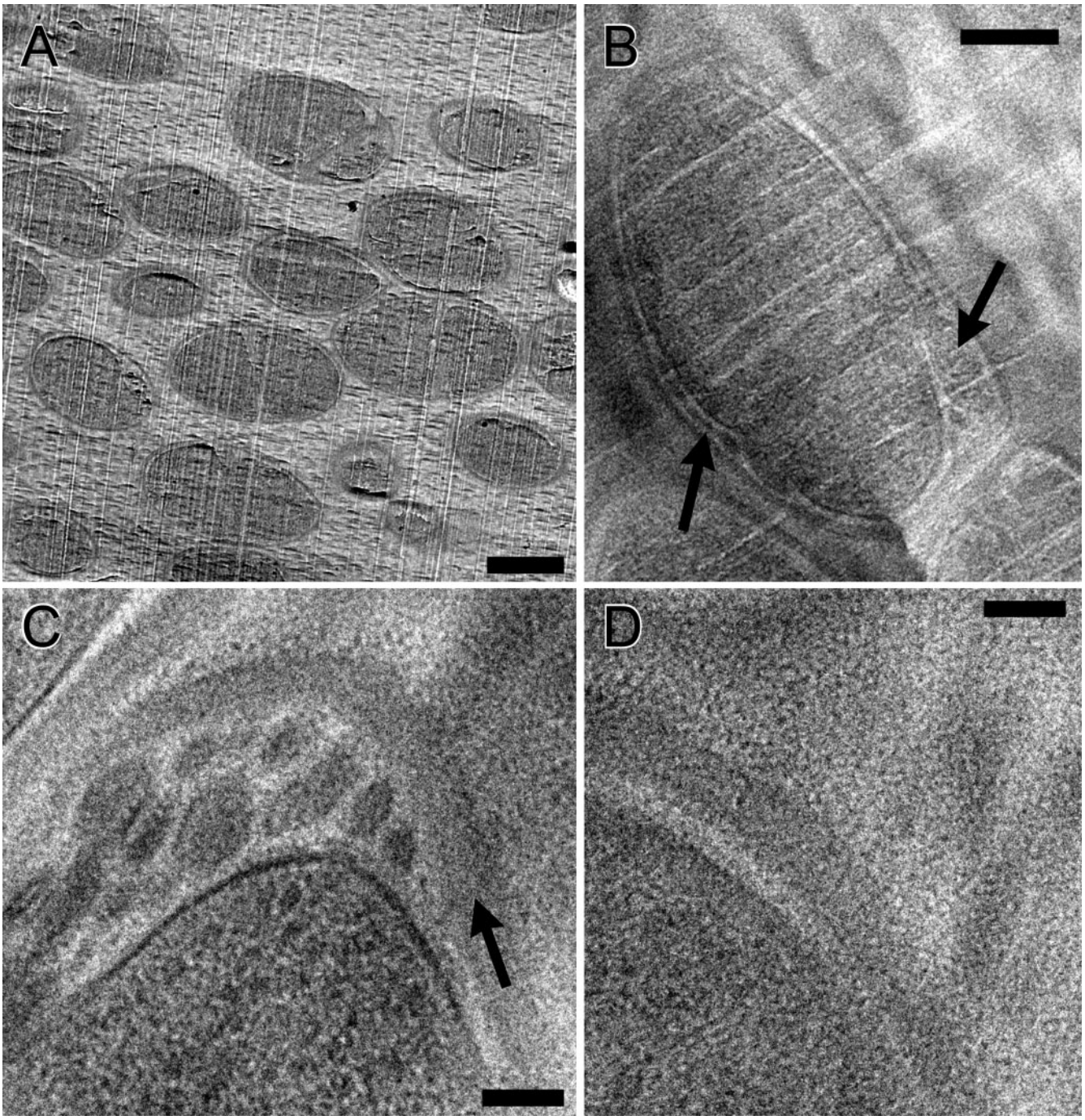

FIG. 6. Plasmolyzed *S. aureus* D_2C cells. (A) Cells show variable separations between the plasma membrane and OWZ. (B) Separation between the OWZ and protoplast is larger at certain regions of the envelope, where membrane vesicles are seen (arrows). (C) Vesicles retaining high-density materials are confined between the membrane and OWZ, which appears thicker than in intact cells (arrow). (D) In areas of the envelope without vesicles, the thickness of the IWZ is similar to that of the IWZs in unplasmolyzed cells, while the OWZ is thicker. Bars, 500 nm (A), 150 nm (B), and 50 nm (C and D).

conditions (from low osmolarities up to a NaCl concentration of 3.5 M [36, 38]). Even with these harsher plasmolysis conditions, *S. aureus* did not undergo plasmolysis as readily as seen previously in *B. subtilis* (30). Plasmolyzed *S. aureus* produced an OWZ that was separated further from the protoplast, which shrank as water was removed from its cytoplasm (Fig. 6A and Table 1). At higher magnification, the IWZ was shown to increase in thickness particularly in certain areas of cells, where membrane vesicles were found between the plasma membrane and OWZ (Fig. 6B). Since plasmolysis causes a considerable reduction of the total area of the membrane associated with the contraction of the protoplast, part of the

TABLE 2. Chemical analyses of *S. aureus* D_2C cell wall fragments

Component	Component concn (μg/mg [dry wt] of wall)[a]		
	Cell wall fragments	Teichoic acid-extracted wall fragments	Protein-and-teichoic acid-extracted walls
Phosphorus	21.21 ± 0.46	1.32 ± 0.18	1.28 ± 0.20
Muramic acid	94 ± 29	151 ± 32	200 ± 24
Aspartic acid	2.5 ± 0.8	6.9 ± 2.2	0.7 ± 0.2
Threonine	5.6 ± 2.1	10.3 ± 2.5	1.2 ± 0.4

[a] Values are the averages ± standard deviations of three measurements.

membrane seems to have been excised, generating vesicles outside the protoplast (these resemble the mesosome bodies found after plasmolysis of *Bacillus megaterium* [52]). The observation of vesicles within the IWZ after plasmolysis is similar to the observations in previous *B. subtilis* experiments (30) and implies that this wall zone is composed mostly of soluble low-density constituents (i.e., it possesses soft materials that allow vesicles to expand within it). In addition, this easily achieved, wide separation of the OWZ from the protoplast is consistent with a deformable space, which would expand upon reduction of turgor pressure during plasmolysis (Fig. 6C). Since many membrane-associated lipidated components interact strongly with the wall matrix in gram-positive bacteria (3, 33), it is possible that such membrane-associated enzymes (27), lipoteichoic acids (34), and lipoproteins (43) could aid in removing portions of membrane from the protoplast during shrinking, resulting in the formation of vesicles. Interestingly, in areas lacking vesicles, the thickness of the IWZ remained similar to the thickness in unplasmolyzed cells. This could be related to a tighter bonding between the OWZ and plasma membrane by larger amounts of lipidated wall components (i.e., membrane-bound wall enzymes, lipoteichoic acids, and lipoproteins; Fig. 6D). The thickness of the OWZ increased compared to that of unshocked cells, as expected, since with lower turgor pressures, wall networks expand due to reduction of stress (Fig. 6C and D and Table 1).

Cell wall fragments. To corroborate the plasmolysis data on the constitution of the IWZ and OWZ, crude cell wall fragments were isolated from mechanically broken cells using a Bead Beater. These fragments were boiled in SDS to remove cytoplasmic contaminants and noncovalently bound wall proteins (WP), and they possessed the major wall constituents (i.e., peptidoglycan, teichoic acids, and covalently bound wall proteins; Table 2). As previously seen in *B. subtilis*, sections of cell wall fragments revealed them to be monopartite in contrast to the bipartite view seen on cells (Fig. 7A and B) (30). *S. aureus* wall fragments consisted of a single 33-nm zone showing contrast similar to that of the OWZs of cell envelopes on intact cells (Fig. 7B and Table 1). As these fragments consisted of isolated walls (Fig. 7B and Table 2), this provides strong evidence that the OWZ seen on cells corresponds to the cell wall polymeric network. The IWZ must be composed mostly of soluble components that were washed away during cell wall isolation and SDS boiling. The increase in thickness of wall fragments compared to the thickness of walls of intact cells is consistent with the removal of turgor pressure after mechanical breakage of cells (Table 1), as this causes the relaxation of the peptidoglycan fabric in the absence of stress. This relaxation also increases the density of the (now) unstretched polymers, since it results in smaller spacings between the polymers. As indicated by the plasmolysis experiment, these data strongly suggest that the IWZ is composed of highly deformable and less substantial wall constituents, implying the presence of a periplasmic space confined by both the plasma membrane and OWZ. As a consequence, the outer wall must represent the peptidoglycan-teichoic acid-protein cell wall network.

Sections of isolated walls also showed that fragments retained only partially the shape of cells (Fig. 7A). Cell walls typically provide a rigid exoskeleton responsible for cell shape in bacteria, but this requirement may not be so strict in these cocci, as a spherical geometry would represent the most energetically favored shape. Moreover, a more flexible wall could aid *S. aureus* to better respond to variations in environmental osmolarities, a feature very important for this highly osmotolerant pathogen (22, 50).

Removal of teichoic acids and proteins from wall fragments. Wall fragments were further treated so as to provide information on cell wall organization. Teichoic acid was extracted from wall fragments using trichloroacetic acid, which removed 94% of TA on the basis of phosphorous analysis (Table 2). TA is responsible for most of the wall's anionic charge due to its abundance and the presence of phosphate groups at both the linkage and repeat units of the polymer (10, 13, 34). TA-extracted walls were composed of predominantly peptidoglycan and wall-bound proteins (Table 2) and, similar to untreated cell wall fragments, had a monopartite appearance (Fig. 7D). Yet, they were more pliable and little cellular shape was left (cf. Fig. 7A and C).

TA-extracted walls were subsequently incubated with a protease to remove most of the covalently bound wall proteins, and these walls were essentially composed of only peptidoglycan (Table 2). WP can be abundant components of walls, particularly in gram-positive cocci. Protein A alone accounts for 7% of the wall content (dry weight) in *S. aureus* (3, 40). Reduction in the concentrations of aspartic acid and threonine, used as protein markers in the cell wall, showed that 90% of wall-bound proteins were removed from these wall fragments (Table 2). Removal of proteins from TA-extracted walls

FIG. 7. *S. aureus* cell wall fragments. (A) Cell wall fragments obtained from mechanically broken and SDS-boiled fragments, containing all major wall components (i.e., peptidoglycan [PG], TA, and WP), only partially retain the shape of cells. The white arrowhead points to ice crystal contamination. (B) Same specimen as in panel A but at a higher magnification shows only one wall zone similar to the OWZs of intact cells. Black arrowheads point to cracks in the supporting film. (C) TA-extracted walls (possessing PG and WP) have even more pliable forms than cell wall fragments do. Long black arrows point to knife marks. (D) At high magnification, TA-extracted walls also show only one wall zone and lower contrast than cell wall fragments; the white arrow points to a septum coming off an outside wall. (E) WP-and-TA-extracted wall fragments (comprising predominantly PG) lack a defined shape. (F) At high magnification, wall fragments stripped of WP and TA show the least contrast and are the most pliable of all wall fragments. Bars, 500 nm (A, C, and E) and 50 nm (B, D, and F).

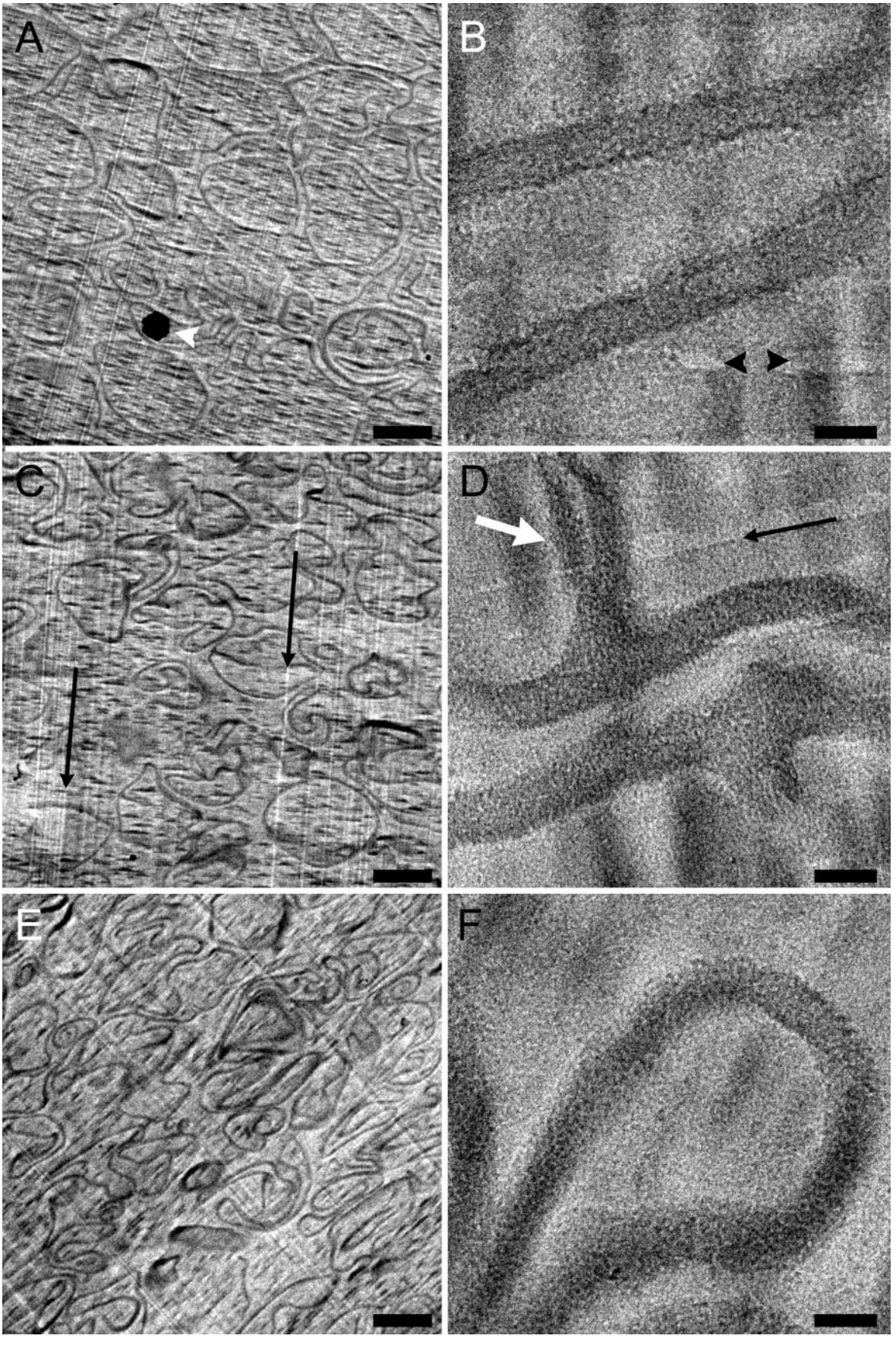
A
B
C
D
E
F

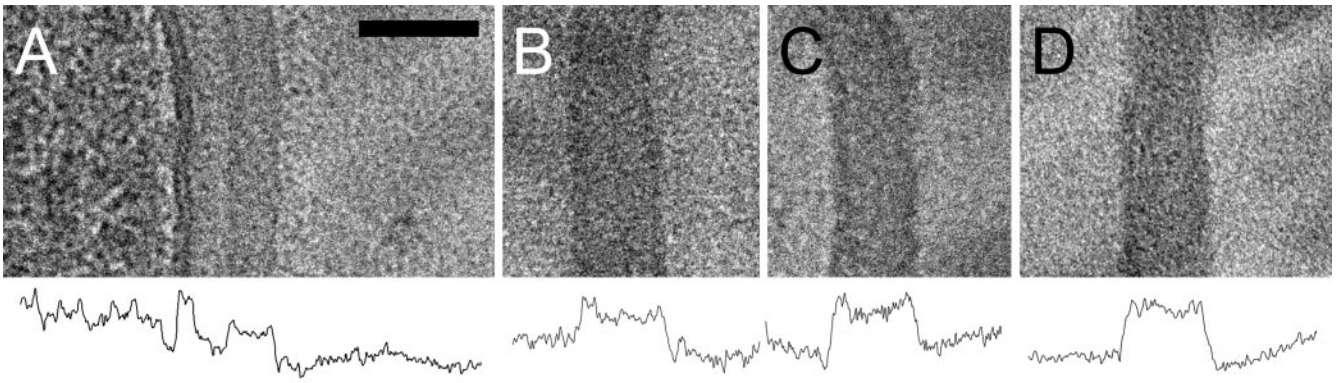

FIG. 8. High-magnification images of *S. aureus* D_2C with the corresponding density tracings. (A) Cell envelope. (B) Cell wall fragments. (C) Teichoic acid-extracted walls. (D) Protease-digested and teichoic acid-extracted walls. Bar, 50 nm.

had a significant influence on the shape and rigidity of walls, and WP-and-TA-extracted wall fragments were still monopartite, with very pliable forms (Fig. 7E and F).

The progressive loss of shape and rigidity after extraction of TA and WP point to an important role for both on wall rigidity in staphylococci (Fig. 7A, B, and C). It is possible that ionic and hydrophobic interactions among peptidoglycan, TA, and WP are especially important in the direction perpendicular to the wall's thickness and increase the wall's stiffness. Since secondary wall components interdigitate with peptidoglycan polymers as they span the wall, their removal could result in wall expansion and loss of rigidity. Interestingly, wall thickness was the same in all three fractions of wall fragments (Table 1). Although the presence of TA and proteins seemed to aid in restricting wall bending, they both had negligible influence on the expansion of the wall thickness. This indicates that secondary polymer bonding is not important in maintaining a constant wall thickness in cells and that the bonding between peptidoglycan polymers is more important. Yet, large forces due to turgor pressure can extend peptidoglycan components laterally, thereby causing contraction of wall thickness. Moreover, the continuous monopartite view seen with all wall fragments provides evidence that TA and WP are not segregated to a particular region of the wall.

Density tracings of the cell envelope and cell walls. Densitometry plots provided information on the distribution of mass through the thickness of walls. Density tracing of the cell envelope showed that the OWZ possessed a relatively constant density along the wall thickness, with similar densities at both the wall's inner and outer surfaces (Fig. 8A). The OWZ also appeared very similar in the three types of wall fragments (Fig. 8B to D), providing more evidence that the OWZ is the peptidoglycan-TA-WP cell wall matrix and that TA and WP are evenly distributed throughout the wall thickness.

The constant density across the wall thickness of this gram-positive bacterium seems to be inconsistent with the concept that peptidoglycan fibers are more stretched at the inner zone because of turgor pressure and their closer proximity to the membrane (17). The *S. aureus* sacculus is composed of very short peptides (six disaccharide units long [6]) and has one of the highest degrees of cross-linking among bacterial peptidoglycans, on the order of 80 to 90% (14). Since this peptidoglycan is a highly cross-linked network of small building blocks, this organism has pliable walls (observed in frozen sections of isolated walls; Fig. 7). Turgor is high in this organism (about 25 to 30 atm) and should stretch the peptidoglycan fibers throughout the thickness of the cell wall. Stretching must affect "relaxed" polymer density by decreasing it. If the cell wall had different in situ densities or if certain regions of the wall were stretched differently by turgor pressure, our technique would distinguish it. No different densities were seen as indicated by the constant levels of density within the wall observed in the density tracing of the cell envelope (Fig. 8A). If the inner region of the wall was the one bearing most of the stress caused by turgor pressure, one would expect a gradual increase in density from inside to outside of the wall, which is not observed. Therefore, the hypothesis that the IWZ represents stretched wall is not valid.

The densitometry plots of the OWZ and wall fragments also showed similar density values on both sides of the wall (Fig. 8A to D), which adds to the notion that turnover of walls in *S. aureus* is mainly localized to the septum. Here, new wall polymers are laid down as the septum grows, and once the septum is completed and daughter cell separation commences, autolytic action splits the septum to release the two new daughter cells (Fig. 8A to D). In other systems (such as in the preexisting cylindrical walls of *B. subtilis*) that require the input of new polymers and the shedding of old polymers by turnover, there exists an inside-to-outside mode of wall growth, which is reflected by a decay of wall density from inside to outside (Fig. 9) (30).

Septation. At the *S. aureus* septum, where most of the wall synthesis takes place, density tracings showed five alternating zones of low and high densities (Fig. 10). The structure of the two zones adjacent to the membrane at the septum compared well to the wall organization of the cell envelope (cf. Fig. 5A and 10). In both cases, a low-density zone was seen above the membrane with a higher density zone above it. The low-density zone next to the membrane appeared to be an extension of the IWZ (Fig. 5B). The high-density zones appeared to be similar to the OWZ, showing a nearly constant level of density throughout the wall thickness (Fig. 10).

In sections of conventionally embedded and freeze-substituted *S. aureus*, a highly stained midline is seen at the septum (15, 44). This midline has been attributed to a splitting system, presumably

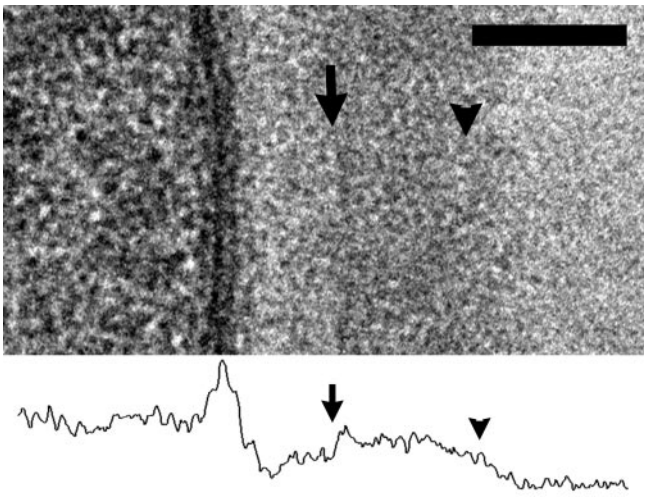

FIG. 9. High-magnification image of the *B. subtilis* envelope with corresponding density tracing. Progressive decrease in the wall density from inside (arrow) to outside (arrowhead) is consistent with the concept of wall turnover. This was not seem in the *S. aureus* cell wall (Fig. 8A). Bar, 50 nm.

involved in cell separation and consisting of concentrically arranged rings of wall substance (15). Our current cryo-TEM results showed that the middle zone of the cross wall possesses low density and has no discernible structure inside. The low-density middle zone of the cross wall resembled the other two low-density regions (IWZs) and could hold similar components, such as penicillin-binding proteins (PBPs) and other enzymes involved in the wall synthesis and hydrolysis.

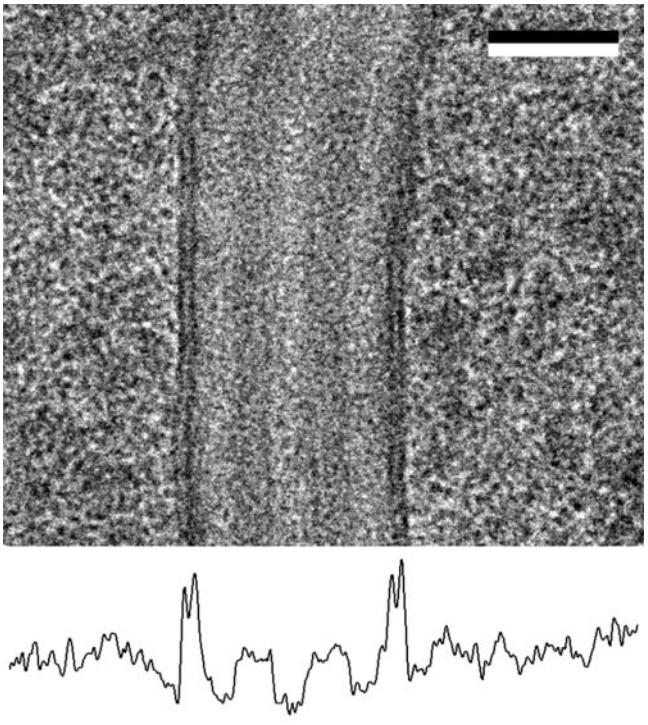

FIG. 10. Density tracing of an *S. aureus* septum at the center of a cell. Two high-density zones are seen sandwiched between three zones of low density. Bar, 50 nm.

DISCUSSION

In this paper we present the cell wall organization of *S. aureus* as revealed by cryo-TEM of frozen-hydrated sections. The plasma membrane was found bound by a bipartite wall, consisting of a low-density 16-nm IWZ, followed by a 19-nm OWZ of higher density. This arrangement was found around cells and extended into the septum, where another low-density zone appeared between the two high-density zones. Our data strongly suggest that, as with *B. subtilis* (30), the IWZ is a periplasmic space, whereas the OWZ consists of the peptidoglycan-teichoic acid cell wall network with its associated proteins. Although suggested before (44, 47), this is the first time strong evidence supports the existence of a periplasmic space in *S. aureus*. This report has shown the following. (i) The IWZ possessed lower density than the OWZ. (ii) Membrane blebs were found in plasmolyzed cells between the protoplast and the OWZ. (iii) Cell wall fragments possessed only one zone of high density similar to that of the OWZ. (iv) The density profile of OWZ was very similar to the profiles of all isolated wall fragments. (v) Wall fragments were thicker than the OWZ after reduction and removal of turgor in plasmolyzed cells and cell wall fragments.

By analogy with gram-negative bacteria, the periplasmic space represents an extraprotoplasmic compartment confined between the plasma membrane and an outer structure (outer membrane versus a peptidoglycan-teichoic acid-protein network), and its constituent periplasm is composed mostly of highly deformable, low-density, soluble components (18, 30). Such a compartment in gram-positive bacteria would represent an advantageous strategy used by these bacteria to provide sufficient space for proper functioning and folding of membrane-bound enzymes involved in the synthesis and transport of macromolecules, such as wall components, exoenzymes, and secreted proteins, situated away from the highly anionic cell wall matrix (27, 28). It is intriguing how gram-positive bacteria maintain a separation between the membrane and the wall fabric, since turgor is of the order of 20 to 30 atm in these bacteria (3, 22). Although the exact mechanism for maintaining their periplasmic space has yet to be elucidated, our plasmolysis results showed stronger bonding between the membrane and wall fabric in certain areas of the envelope, implying that membrane-bound polymers, which interact with the wall (i.e., PBPs, lipoteichoic acids, lipoproteins [3, 27, 34, 43]), could form a scaffolding that keeps the wall away from the protoplast.

The frozen-hydrated profile of the *S. aureus* cell envelope appears markedly different from the tripartite wall seen by freeze-substitution, but one should remember that contrast is achieved in different ways by each technique. Freeze-substitution uses heavy metal stains to make visible structures with metal binding ability, whereas in frozen-hydrated sections, contrast is proportional to the mass of the structural component. Accordingly, frozen-hydrated sections show a low-density periplasmic space in the cell envelope, which appears heavily stained in freeze-substituted specimens because of the high heavy metal affinity of the periplasm, similar to what is ob-

served in gram-negative bacteria (29). The thickness of the frozen-hydrated cell wall matrix compared reasonably well with the translucent wall revealed by freeze-substitution (region 2 [Fig. 2]), and these walls show constant mass and constant metal binding throughout their thickness. However, preservation of the plasma membrane and periplasm seems remarkably better achieved in frozen-hydrated sections, which shows bilayered membranes and a much wider periplasmic space. Admittedly, it is still possible that the cryoprotectant used in this study and required to vitrify samples could have had subtle effects on the sizes of wall structures. The only feature not seen in frozen-hydrated *S. aureus* walls was the highly stained surface fringe of freeze-substituted cells which has been suggested to consist mostly of teichoic acids (47). This identification is based on the results of immunolabeling experiments that labeled most of the wall outer surface using nanogold particles, which give limited resolution due to particle size (5 to 10 nm [47]). Our results give no indication of segregation of teichoic acids in the wall fabric, as wall fragments possessed the same thickness before and after extraction of teichoic acids and density tracings of the OWZ and all wall fragments showed an almost constant density over the thickness of walls. It is probable that whatever is on the surface of the wall possesses high metal binding ability and lower local density than the outer medium (10% glycerol in our frozen-hydrated sections) and does not provide enough contrast for cryo-TEM (which uses differential mass for imaging).

Despite the optimal structural preservation assured by vitrification, the molecular organization of the wall components within the wall fabric could not be discerned in our frozen-hydrated sections. Their visualization is certainly a very challenging task because of the gel-like and heterogeneous nature of the wall, attested to by many high-resolution techniques (e.g., X-ray scattering, TEM of isolated walls, and atomic force microscopy [8, 24, 46]). Accordingly, many models have been proposed to describe the tertiary structure of peptidoglycan. In the most traditional view, growing glycan strands (bearing stem peptides and oriented parallel to the membrane) are incorporated into the wall, forming a multilayered peptidoglycan thick enough to withstand turgor pressures of the order of 25 atm (23, 24, 51). A recent "scaffold" model of murein architecture, which depicts glycan strands as oriented perpendicularly to the plasma membrane, has been proposed for the *S. aureus* peptidoglycan tertiary structure, and the degree of cross-linking seems to reflect experimental data better (9). The frozen-hydrated data on *S. aureus* cannot distinguish between the "parallel to membrane"' (horizontal) and "scaffolding" (vertical) models.

Division of *S. aureus* could be observed in frozen-hydrated sections. *S. aureus* septa possessed five distinct zones of different densities, but the two zones adjacent to the membrane seemed to be an extension of the envelope. The middle zone of the cross wall had low density with no distinguishing structures within it and could, like the periplasmic space, consist of soluble substances. Presumably, the middle zone has a high heavy metal binding ability, which would result in a heavily stained midline in both conventional and freeze-substituted sections. The use of a heavy metal label specific for PBPs has in fact increased the thickness of this midline, suggesting the presence of PBPs at this region of the septum (35), even though most PBPs must be associated with the membrane. Further work is necessary to unravel the nature of the middle zone of the septum and the complex mechanisms involved in cross wall formation of *S. aureus*.

A view of the intriguing complexity of the staphylococcal cell wall has emerged with the use of cryo-TEM of frozen-hydrated sections. The existence of a periplasmic space and of a complex architecture at the septum in this pathogen points to elaborate cellular mechanisms of division and cell wall synthesis. Certainly more studies will be necessary to reveal the structural basis involved in the maintenance of a periplasmic space and in cross wall synthesis in gram-positive bacteria, but cryo-TEM of frozen-hydrated sections will be essential to help find these answers.

ACKNOWLEDGMENTS

We thank A. Saxena of our laboratory for technical assistance.

This work was supported by a Natural Science and Engineering Research Council of Canada (NSERC) Discovery grant to T.J.B. V.R.F.M. was the recipient of a Ph.D. scholarship from CNPq/Brazil during part of this study. Microscopy was performed in the NSERC Guelph Regional Integrated Imaging Facility (GRIIF), which is partially funded by an NSERC Major Facility Access grant to T.J.B.

REFERENCES

1. **Amako, K., A. Umeda, and K. Murata.** 1982. Arrangement of peptidoglycan in the cell wall of *Staphylococcus* spp. J. Bacteriol. **150:**844–850.
2. **Amako, K., and A. Umeda.** 1979. Regular arrangement of wall polymers in staphylococci. J. Gen. Microbiol. **113:**421–424.
3. **Archibald, A. R., I. C. Hancock, and C. R. Harwood.** 1993. Cell wall structure, synthesis, and turnover, p. 381–410. *In* A. L. Sonenshein, J. A. Hoch, and R. Losick (ed.), *Bacillus subtilis* and other gram-positive bacteria. American Society for Microbiology, Washington, D.C.
4. **Beveridge, T. J., and V. R. F. Matias.** Ultrastructure of gram-positive cell walls. *In* V. A. Fischetti, R. P. Novick, J. J. Ferreti, D. A. Portnoy, and J. I. Rood (ed.), Gram-positive bacteria, 2nd ed., in press. American Society for Microbiology, Washington, D.C.
5. **Beveridge, T. J., D. Moyles, and B. Harris.** Electron microscopy. *In* C. A. Reddy, T. J. Beveridge, et al. (ed.), Methods for general and molecular microbiology, in press. American Society for Microbiology, Washington, D.C.
6. **Boneca, I. G., Z. H. Huang, D. A. Gage, and A. Tomasz.** 2000. Characterization of *Staphylococcus aureus* cell wall glycan strands, evidence for a new β-*N*-acetylglucosaminidase activity. J. Biol. Chem. **275:**9910–9918.
7. **Clarke, A. J.** 1993. Compositional analysis of peptidoglycan by high-performance anion-exchange chromatography. Anal. Biochem. **212:**344–350.
8. **Dietrich, I., H. Formanek, F. Fox, E. Knapek, and R. Weyl.** 1979. Reduction of radiation damage in an electron microscope with a superconducting lens system. Nature **277:**380–381.
9. **Dmitriev, B. A., F. V. Toukach, O. Holst, E. T. Rietschel, and S. Ehlers.** 2004. Tertiary structure of *Staphylococcus aureus* cell wall murein. J. Bacteriol. **186:**7141–7148.
10. **Dobson, B. C., and A. R. Archibald.** 1978. Effect of specific growth limitations on cell wall composition of *Staphylococcus aureus* H. Arch. Microbiol. **119:**295–301.
11. **Dubochet, J., A. W. McDowall, B. Menge, E. N. Schmid, and K. G. Lickfeld.** 1983. Electron microscopy of frozen-hydrated bacteria. J. Bacteriol. **155:** 381–390.
12. **Dubochet, J., M. Adrian, J. J. Chang, J. C. Homo, J. Lepault, A. W. McDowall, and P. Schultz.** 1988. Cryo-electron microscopy of vitrified specimens. Q. Rev. Biophys. **21:**129–228.
13. **Fox, K. F., G. C. Stewart, and A. Fox.** 1998. Synthesis of microcapsule by *Staphylococcus aureus* is not responsive to environmental phosphate concentrations. Infect. Immun. **66:**4004–4007.
14. **Gally, D., and A. R. Archibald.** 1993. Cell wall assembly in *Staphylococcus aureus*: proposed absence of secondary crosslinking reactions. J. Gen. Microbiol. **139:**1907–1913.
15. **Giesbrecht, P., T. Kersten, H. Maidhof, and J. Wecke.** 1998. Staphylococcal cell wall: morphogenesis and fatal variations in the presence of penicillin. Microbiol. Mol. Biol. Rev. **62:**1371–1414.
16. **Graham, L. L., and T. J. Beveridge.** 1990. Effect of chemical fixatives on accurate preservation of *Escherichia coli* and *Bacillus subtilis* structure in cells prepared by freeze-substitution. J. Bacteriol. **172:**2150–2159.
17. **Graham, L. L., and T. J. Beveridge.** 1994. Structural differentiation of the *Bacillus subtilis* 168 cell wall. J. Bacteriol. **176:**1413–1421.

18. **Graham, L. L., T. J. Beveridge, and N. Nanninga.** 1991. Periplasmic space and the concept of the periplasm. Trends Biochem. Sci. **16:**328–329.
19. **Hancock, I., and I. Poxton.** 1988. Bacterial cell surface techniques. John Wiley & Sons, Bath Press, Ltd., Chichester, United Kingdom.
20. **Koch, A. L.** 1983. The surface stress theory of microbial morphogenesis. Adv. Microb. Physiol. **24:**301–366.
21. **Koyama, T., M. Yamada, and M. Matsuhashi.** 1977. Formation of regular packets of *Staphylococcus aureus* cells. J. Bacteriol. **129:**1518–1523.
22. **Kunin, C. M., and J. Rudy.** 1991. Effect of NaCl-induced osmotic stress on intracellular concentrations of glycine betaine and potassium in *Escherichia coli*, *Enterococcus faecalis*, and staphylococci. J. Lab. Clin. Med. **118:**217–224.
23. **Labischinski, H., E. W. Goodell, A. Goodell, and M. L. Hochberg.** 1991. Direct proof of a "more-than-a-single-layered" peptidoglycan architecture of *Escherichia coli* W7: a neutron small-angle scattering study. J. Bacteriol. **173:**751–756.
24. **Labischinski, H., G. Barnickel, H. Bradaczek, and P. Giesbrecht.** 1979. On the secondary and tertiary structure of murein: low and medium-angle x-ray evidence against chitin-based conformations of bacterial peptidoglycan. Eur. J. Biochem. **95:**147–155.
25. **Lancette, G. A., and R. W. Bennett.** 2001. *Staphylococcus aureus* and staphylococcal enterotoxins, p. 387–403. *In* F. P. Downes and K. Ito (ed.), Compendium of methods for the microbiological examination of foods. American Public Health Association, Washington, D.C.
26. **Łęski, T. A., and A. Tomasz.** 2005. Role of penicillin-binding protein 2 (PBP2) in the antibiotic susceptibility and cell wall cross-linking of *Staphylococcus aureus*: evidence for the cooperative functioning of PBP2, PBP4, and PBP2A. J. Bacteriol. **187:**1815–1824.
27. **Lim, D., and N. C. J. Strynadka.** 2002. Structural basis for the β-lactam resistance of PBP2a from methicillin-resistant *Staphylococcus aureus*. Nat. Struct. Biol. **9:**870–876.
28. **Marraffini, L. A., H. Ton-That, Y. Zong, S. V. L. Narayana, and O. Schneewind.** 2004. Anchoring of surface proteins to the cell wall of *Staphylococcus aureus*. J. Biol. Chem. **279:**37763–37770.
29. **Matias, V. R. F., A. Al-Amoudi, J. Dubochet, and T. J. Beveridge.** 2003. Cryo-transmission electron microscopy of frozen-hydrated sections of gram-negative bacteria. J. Bacteriol. **185:**6112–6118.
30. **Matias, V. R. F., and T. J. Beveridge.** 2005. Cryo-electron microscopy reveals native polymeric cell wall structure in *Bacillus subtilis* 168 and the existence of a periplasmic space. Mol. Microbiol. **56:**240–251.
31. **Mead, P. S., L. Slutsker, V. Dietz, L. F. McCaig, J. S. Bresee, C. Shapiro, P. M. Griffin, and R. V. Tauxe.** 1999. Food-related illness and death in the United States. Emerg. Infect. Dis. **5:**607–624.
32. **Moor, H., G. Bellin, C. Sandri, and K. Akert.** 1980. The influence of high pressure freezing on mammalian nerve tissue. Cell Tissue Res. **209:**201–216.
33. **Navarre, W. W., and O. Schneewind.** 1999. Surface proteins of gram-positive bacteria and mechanisms of their targeting to the cell wall envelope. Microbiol. Mol. Biol. Rev. **63:**174–229.
34. **Neuhaus, F. C., and J. Baddiley.** 2003. A continuum of anionic charge: structures and functions of D-alanyl-teichoic acids in gram-positive bacteria. Microbiol. Mol. Biol. Rev. **67:**686–723.
35. **Paul, T. R., A. Venter, L. C. Blaszczak, T. R. Parr, Jr., H. Labischinski, and T. J. Beveridge.** 1995. Localization of penicillin-binding proteins to the splitting system of *Staphylococcus aureus* septa by using a mercury-penicillin V derivative. J. Bacteriol. **177:**3631–3640.
36. **Peddie, B. A., J. Wong-She, K. Randall, M. Lever, and S. T. Chambers.** 1998. Osmoprotective properties and accumulation of betaine analogues by *Staphylococcus aureus*. FEMS Microbiol. Lett. **160:**25–30.
37. **Sartori, N., K. Richter, and J. Dubochet.** 1993. Vitrification depth can be increased more than 10 fold by high pressure freezing. J. Microsc. **172:**55–61.
38. **Scott, W. J.** 1953. Water relations of *Staphylococcus aureus* at 30°C. Aust. J. Biol. Sci. **6:**549–564.
39. **Sieradzki, K., and A. Tomasz.** 2003. Alterations of cell wall structure and metabolism accompany reduced susceptibility to vancomycin in an isogenic series of clinical isolates of *Staphylococcus aureus*. J. Bacteriol. **185:**7103–7110.
40. **Sjöquist, J., J. Movitz, I. B. Johansson, and H. Hjelm.** 1972. Localization of protein A in the bacteria. Eur. J. Biochem. **30:**190–194.
41. **Sprott, G. D., S. F. Koval, and C. A. Schnaitman.** 1994. Cell fractionation, p. 72–103. *In* P. Gerhardt, R. G. E. Murray, W. A. Wood, and N. R. Krieg (ed.), Methods for general and molecular bacteriology. American Society for Microbiology, Washington, D.C.
42. **Studer, D., W. Graber, A. Al-Amoudi, and P. Eggli.** 2001. A new approach for cryofixation by high-pressure freezing. J. Microsc. **203:**285–294.
43. **Sutcliffe, I. C., and R. R. B. Russel.** 1995. Lipoproteins of gram-positive bacteria. J. Bacteriol. **177:**1123–1128.
44. **Takade, A., A. Umeda, S. Yokoyama, and K. Amako.** 1988. The substitution-fixation of *Staphylococcus aureus*. J. Electron Microsc. **37:**215–217.
45. **Tomasz, A.** 2000. The staphylococcal cell wall, p. 351–360. *In* V. A. Fischetti, R. P. Novick, J. J. Ferreti, D. A. Portnoy, and J. I. Rood (ed.), Gram-positive bacteria. American Society for Microbiology, Washington, D.C.
46. **Touhami, A., M. H. Jericho, and T. J. Beveridge.** 2004. Atomic force microscopy of cell growth and division in *Staphylococcus aureus*. J. Bacteriol. **186:**3286–3295.
47. **Umeda, A., S. Yokoyama, T. Arizono, and K. Amako.** 1992. Localization of peptidoglycan and teichoic acid on the cell wall surface of *Staphylococcus aureus* as determined by immunoelectron microscopy. J. Electron Microsc. **41:**46–52.
48. **Umeda, A., T. Ikebuchi, and K. Amako.** 1980. Localization of bacteriophage receptor, clumping factor, and protein A on the cell surface of *Staphylococcus aureus*. J. Bacteriol. **141:**838–844.
49. **Umeda, A., Y. Ueki, and K. Amako.** 1987. Structure of the *Staphylococcus aureus* cell wall determined by the freeze-substitution method. J. Bacteriol. **169:**2482–2487.
50. **Vijaranakul, U., M. J. Nadakavukaren, B. L. M. de Jonge, B. J. Wilkinson, and R. K. Jayaswal.** 1995. Increased cell size and shortened peptidoglycan interpeptide bridge of NaCl-stressed *Staphylococcus aureus* and their reversal by glycine betaine. J. Bacteriol. **177:**5116–5121.
51. **Vollmer, W., and J. V. Höltje.** 2004. The architecture of the murein (peptidoglycan) in gram-negative bacteria: vertical scaffold or horizontal layer(s)? J. Bacteriol. **186:**5978–5987.
52. **Weibull, C.** 1965. Plasmolysis in *Bacillus megaterium*. J. Bacteriol. **89:**1151–1154.
53. **Yamada, S., M. Sugai, H. Komatsuzawa, S. Nakashima, T. Oshida, A. Matsumoto, and H. Suginaka.** 1996. An autolysin ring associated with cell separation of *Staphylococcus aureus*. J. Bacteriol. **178:**1565–1571.
54. **Zhang, P., E. Bos, J. Heymann, H. Gnaegi, M. Kessel, P. J. Peters, and S. Subramaniam.** 2004. Direct visualization of receptor arrays in frozen-hydrated sections and plunge-frozen specimens of *E. coli* engineered to overproduce the chemotaxis receptor Tsr. J. Microsc. **216:**76–83.